



OPEN

## Kinetic study of Fe & Co perovskite catalyst in Fischer–Tropsch synthesis

Behnoosh Moshtari, Seyed Hasan Hashemabadi✉ &amp; Yahya Zamani

The investigation of the reaction's kinetics is one of the most crucial aspects of the design of a commercial process. The current research investigates the kinetics of Fischer–Tropsch synthesis using a perovskite catalyst. The  $\text{LaFe}_{0.7}\text{Co}_{0.3}\text{O}_3$  perovskite catalyst was prepared via the thermal sol–gel technique and characterized using BET, XRD, SEM, and  $\text{H}_2$ -TPR techniques. According to operating conditions (e.g.  $\text{H}_2/\text{CO}$ : 1–2, pressure: 10–20 barg, temperature: 240–300 °C, and GHSV: 3000 1/h), Fischer–Tropsch reaction kinetics (CO conversion) were carried out in a fixed-bed reactor. Using the framework of Langmuir–Hinshelwood–Hougen–Watson (LHHW) theories, 18 kinetic expressions for CO conversion were derived, and all were fitted to experimental data one by one to determine the optimum condition. The correlation was derived from experimental data and well-fitted using LHHW form (according to the enol mechanism, carbon monoxide and dissociated hydrogen atoms are adsorbed and reacted on the surface of the catalyst)  $-r_{\text{CO}} = k_p b_{\text{CO}} P_{\text{CO}} (b_{\text{H}_2} P_{\text{H}_2})^{0.5} / (1 + b_{\text{CO}} P_{\text{CO}} + (b_{\text{H}_2} P_{\text{H}_2})^{0.5})^2$ . Finally, the activation energy of the optimum kinetic model was determined with respect to the Arrhenius equation under various operating conditions. The activation energy of perovskite catalyst is about 106.25 kJ/mol at temperatures 240–300 °C, pressures 10–20 barg, and  $\text{H}_2/\text{CO}$  ratios 1–2, which is lower than other types of catalyst. Therefore, the catalyst was activated at a high temperature and demonstrated stable performance without any temperature runaway and coking issues.

**Keywords** Fischer–Tropsch synthesis, Perovskite catalyst, Kinetic model

### List of symbols

$a$	Adsorption parameter
$b$	Adsorption parameter
$C_V$	Free active sites
$d$	Mean size of crystal
$E$	Activation energy (kJ/mol)
$F_{\text{CO}}$	Molar flow rate of CO at the inlet ( $\text{mol min}^{-1}$ )
$K$	Dimensionless shape factor
$k$	Reaction rate constant
$N$	Number experimental data points
$P_{\text{CO}}$	CO pressure (bar)
$P_{\text{H}_2}$	Hydrogen pressure (bar)
$-r_{\text{CO}}$	The consumption rate of CO ( $\text{mol/g}_{\text{cat}} \text{ min}$ )
$-R_{\text{FT}}$	Rate of reaction ( $\text{mol/g}_{\text{cat}} \text{ min}$ )
$W$	Catalyst mass (gr)
$x$	Conversion
$\beta$	Line broadening at half the maximum intensity (FWHM)
$\lambda$	Is the X-ray wavelength

### Superscripts

$exp$	Experimental value
$cal$	Predicted value

CFD Research Laboratory, School of Chemical Engineering, Iran University of Science and Technology, Narmak, Tehran, Iran. ✉email: hashemabadi@iust.ac.ir

Fischer–Tropsch synthesis (FTS) is a series of polymeric reactions for converting syngas (a mixture of CO and H<sub>2</sub>) to liquid hydrocarbons<sup>1–3</sup>. The high growth of the world's population and the advancement of technology have led to an increase in the demand for liquid fuels; consequently, this process is regarded as a viable alternative for producing valuable fuels<sup>4–6</sup>. Hydrocarbons with FTS are considered clean fuels due to their low sulfur content<sup>7</sup>. FT process is regarded as a catalytic process. Metals in the 8–10 group are the most effective catalysts for Fischer–Tropsch synthesis, and among them, Iron and cobalt have demonstrated superior performance compared to other metals. Due to the exothermic nature of the reactions in the FT process, catalyst efficiency reduces accordingly. Therefore, the yield of desirable products decreases due to the resistance of the catalyst to a sudden increase in temperature; thus the behavior of the catalyst at the beginning of the reaction is crucial. Perovskite catalysts have been popular in recent years due to their high thermal stability and diverse performance<sup>7,8</sup>. The general structure of the perovskite catalysts is ABO<sub>3</sub>, in which A and B are metal groups and A is a larger cation than B<sup>8–10</sup>. Furthermore, investigating the kinetic is one of the most important topics for designing commercial processes. Therefore, many researchers are interested in developing a kinetic model for the FT process with a wide range of operating conditions<sup>11,12</sup>. There have been numerous attempts to define the FT process's kinetics, and there are many kinetic models. All the developing models can be classified into 4 categories: Power Low (PL), Eley-Raidal (ER), Langmuir Hinshelwood Hugon Watson (LHHW), and Termolecular (TM)<sup>13–16</sup>. Anderson, Dry and Yates suggested the first kinetic equations for Fischer Tropsch synthesis, and it was widely used by other researchers<sup>17–19</sup>. Boots et al. studied the kinetic equations for Fe and Co catalysts in various operating conditions. They proved that the empirical results demonstrate a significant deviation from model equations. They reported new kinetic equations (Table 1)<sup>20,21</sup>. In 2010 Ojeda et al.<sup>22</sup> investigated the kinetics of Fischer-Trosch synthesis using iron and cobalt catalysts. They stated that the same mechanism could explain the kinetic model of Iron and cobalt, and finally, they developed a single equation for both catalysts (Table 1). Although the actual partial pressure of hydrogen is zero, their predicted model is not zero; therefore, it is not acceptable<sup>22</sup>. Nikbakht et al.<sup>23</sup> reported the catalyst performance along with the kinetic of hydrocarbon-formation reactions for a Fe-Co-Ce catalyst on zeolite support in a fixed bed reactor. They developed the best-fitted model and obtained the kinetic parameters for CO consumption with/without the water term. Einbeigi et al. investigated the kinetics and mechanisms of Fischer–Tropsch synthesis over a %10Fe/%10Co/%80 γ-Al<sub>2</sub>O<sub>3</sub> nanocatalyst prepared by the impregnation method in a fixed bed micro-reactor<sup>24</sup>. In 2023, Yahyazadeh et al. evaluated the kinetics of the FT reaction with a KMo bimetallic-promoted Fe catalyst supported on carbon nanotubes (CNTs)<sup>25</sup>. Although there are many studies on the kinetic models of Fischer–Tropsch synthesis using Fe or Co as an active site with various supporters (e.g. γ-alumina or TiO<sub>2</sub>), few studies have been carried out on the kinetic models of perovskite catalysts. Due to high thermal stability and low deactivation rate, perovskite catalysts have been noticed recently. Therefore, the current research focused on the kinetic and mechanism of Fischer–Tropsch based on perovskite catalyst; that is the LaFe<sub>0.7</sub>Co<sub>0.3</sub>O<sub>3</sub> perovskite catalyst is prepared, characterized and tested in a fixed bed reactor.

## Material and methods

### Materials

All materials were used as received: Iron (III) nitrate (Fe(NO<sub>3</sub>)<sub>3</sub>·9H<sub>2</sub>O, Merck, 98%), Cobalt (II) nitrate (Co(NO<sub>3</sub>)<sub>2</sub>·6H<sub>2</sub>O, Merck, 99%), Lanthanum(III) nitrate (La(NO<sub>3</sub>)<sub>3</sub>·6H<sub>2</sub>O, Merck, 99%), Glycine (NH<sub>2</sub>CH<sub>2</sub>COOH, Merck, 99%). The deionized water was applied for catalyst synthesis.

### Methods

#### Catalyst preparation

There are various methods for preparing perovskite oxide such as hydrothermal, microwave, precipitation, sol–gel, etc.<sup>26</sup>. The La Fe<sub>0.7</sub>Co<sub>0.3</sub>O<sub>3</sub> perovskite catalyst was prepared using the thermal sol–gel method. The catalyst was synthesized at room temperature by an aqueous solution of La(NO<sub>3</sub>)<sub>3</sub>·6H<sub>2</sub>O, Co(NO<sub>3</sub>)<sub>2</sub>·6H<sub>2</sub>O, and Fe(NO<sub>3</sub>)<sub>3</sub>·9H<sub>2</sub>O, then glycine solution was added drop wise to form the gel<sup>27,28</sup>. The prepared gel was dried at 180 °C for 4 h in the oven, and then calcinated in a furnace at 550 °C (5 °C/min) for 5 h. The sample was pressed into pellets, crushed, and sieved to obtain particles in size between the 40–60 ASTM mesh.

Equation	catalyst	Type	Ref
$A P_{H_2}^{0.5} P_{CO}^{-0.2}$	Co/Al <sub>2</sub> O <sub>3</sub>	PL	13
$A \frac{P_{H_2}^{0.5} P_{CO}^{-0.25}}{1 - k_1 \left( \frac{P_{H_2} O}{P_{H_2}} \right)}$	Co/SiO <sub>2</sub>	ER	14
$A \frac{P_{H_2} P_{CO}^{0.5}}{(1 + k_1 P_{CO}^{0.5})^2}$	Co/Al <sub>2</sub> O <sub>3</sub>	TM	15
$\frac{k P_{CO} P_{H_2}}{(1 + a P_{H_2}^{0.5} + b P_{CO} P_{H_2}^{0.5})^2}$	Co/MnO <sub>4</sub>	LHHW	16
$\frac{A P_{H_2} P_{CO} + B P_{CO}}{(1 + k_1 P_{CO})^2}$	Fe,Co/K,Cu	LHHW	22

**Table 1.** Most cited Fischer–Tropsch reaction rate equations.

### Catalyst characterization

The XRD measurement was carried out using the Philips PW1729 system. The diffraction pattern was obtained using a CuK $\alpha$  lamp with wavelength  $\lambda = 1.542\text{\AA}$  in the angle range  $2\theta = 1$  to  $2\theta = 80$  and a step size of 0.06. The size of the particle crystals is calculated based on the XRD information and using the Scherer equation.

Brunner Emmett Teller (BET) surface area, pore volume and mean pore diameter of the catalyst were determined using an ASAP 3020 instrument of Micrometrics. The SEM images were recorded using MIRA3 Tescan. Temperature Programmed Reduction (TPR) was carried out on 0.011 g of catalyst heated from 28 to 750 °C (20 °C/min) under 5% H<sub>2</sub> in Argon (total gas flow: 50 Ncc/min) with Chembet 3000 system. A CM120 microscope manufactured by Philips did the Transmission Electron Microscopy (TEM) test on the catalysts.

### Catalyst activity measurement

The kinetic tests were performed in a fixed bed reactor using LaFe<sub>0.7</sub>Co<sub>0.3</sub>O<sub>3</sub> catalyst for Fischer Tropsch synthesis. The reactor was made of stainless steel with an 8 mm diameter and 700 mm height. The amount of 1 g catalyst is loaded into one-third of the reactor. The set-up consisted of 3 units: a feeding unit, a reaction unit, and a product separation and analysis unit. Figure 1 shows the schematic of the FT set-up.

The catalyst performance was tested under pressure and temperature ranges of 10–20 bar and 240–300 °C, respectively. The feed consisted of carbon monoxide and hydrogen with a percentage of 50% and 50%, respectively. The experimental results are reported in Table 3. The reactor temperature is controlled by a furnace equipped with a temperature controller located around the reactor to maintain a uniform temperature. To prevent choking of the reactor's outlet in case of the formation of heavy hydrocarbons, the reactor system is equipped with two hot and cold traps to collect light and heavy liquid products. The liquid products are discharged from the traps and gas products are sent to the GC (Agilent 7890) by a stainless steel tube. The feed has three mass flow controllers (MFCs): hydrogen, carbon monoxide, and nitrogen gases. The feed was preheated prior to entering the reactor. The reactor's pressure is adjusted using a pressure valve (Groove) installed before the outlet (Fig. 1).

After loading the catalyst in the reactor, to reduce the catalyst, the mixture of hydrogen and nitrogen gases with a ratio of 1 to 10 (H<sub>2</sub> / N<sub>2</sub> = 1/10) under atmospheric pressure at 450 °C for 24 h passes throughout the catalyst bed. However, developing kinetic equations requires a series of experiments in specific operating conditions. The intrinsic rate equations were estimated by comparing the theoretical and experimental rates. To determine the kinetic equation in a fixed bed reactor, several factors should be considered as follows<sup>19,29,30</sup>:

- Catalyst activity should not be reduced.
- The temperature of the reactor should be constant (Due to the exothermic nature of the Fischer reaction, the operating conditions of the reaction should be considered in such a way that the CO conversion is low.)
- No mass transfer limitation is implied in the calculations.

However, to determine the kinetic equation under laboratory conditions, the velocity must be assumed to be uniform along the length of the reactor. Regarding the above assumption, the operating conditions should be

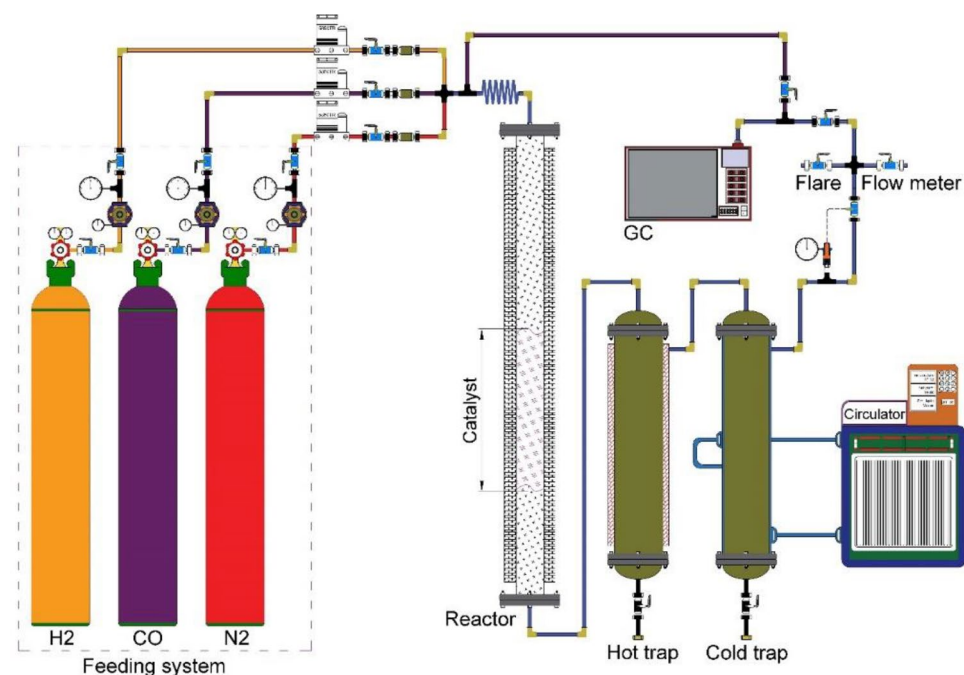


**Figure 1.** Schematics of the Fischer–Tropsch Set-up.

implemented in such a way that the CO conversion becomes less than 15%. In these situations, the reaction rate through the reactor is constant and the following equation can be used:

$$\frac{W}{F_{CO}} = \int_{x_{in}}^{x_{out}} \frac{dx}{-r_{CO}} = \frac{X_{out} - X_{in}}{-r_{CO}} \quad (1)$$

The average rate is:

$$-r_{CO} = \frac{x_{CO}F_{CO}}{W} \text{ or } -r_{CO} = r_{CO(in)} - r_{CO(out)} \quad (2)$$

In order to simplify the kinetics equations, the mass transfer resistance was relinquished from calculations. According to the ideal gas law the partial pressure of each component calculated as blow:

$$P_{CO} = X_{CO} * P_{total} \quad (3)$$

$$P_{H_2} = X_{H_2} * P_{total} \quad (4)$$

## Result and discussion

### Catalyst characterization results

The X-ray diffraction (XRD) of the prepared  $\text{LaFe}_{0.7}\text{Co}_{0.3}\text{O}_3$  is presented in Fig. 2a. The catalyst was calcinated at 550 °C and XRD determined the crystal structure. According to Fig. 2 the diffraction peaks of the perovskite structure in the range of  $2\theta = 30\text{--}40$  are sharpened, and it is proved that the perovskite structure was formed. The used catalyst was characterized using XRD technique to identify the changes in its structure (Fig. 2b). The size of the  $\text{LaFe}_{0.7}\text{Co}_{0.3}\text{O}_3$  crystals was calculated according to X-ray diffraction data with Scherer's equation<sup>31</sup>:

$$d = \frac{K\lambda}{\beta \cos\theta} \quad (5)$$

Scherer modified another correlation to calculate the size of crystals<sup>31</sup>:

$$\ln\beta = \ln\frac{k\lambda}{L} + \ln\frac{1}{\cos\theta} \quad (6)$$

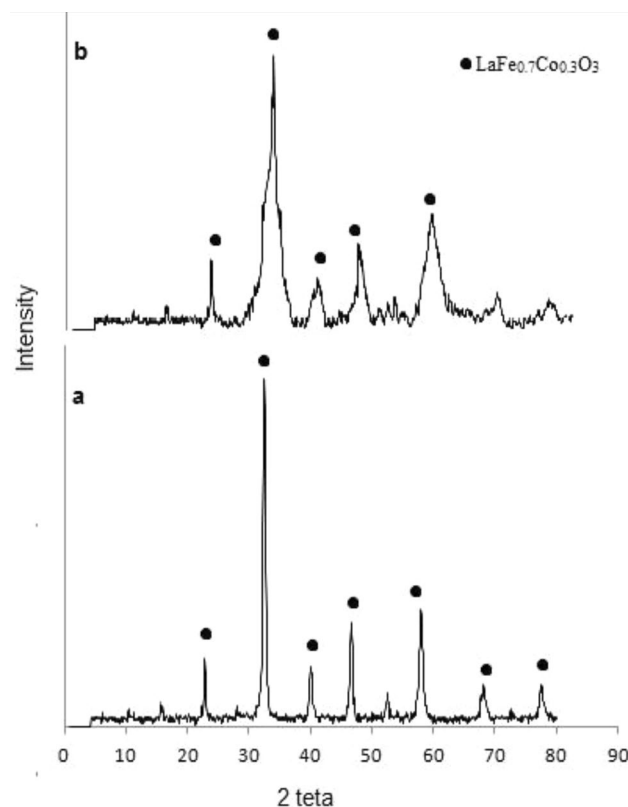


**Figure 2.** XRD Pattern (a) fresh catalyst (b) used catalyst.

According to Scherer's equation, the average particle size was 30.69. The  $\ln(\beta)$  vs.  $\ln(1/\cos\theta)$  line graph was depicted for the  $\text{LaFe}_{0.7}\text{Co}_{0.3}\text{O}_3$  crystals using the modified Scherer correlation (Fig. 3). According to the correlation, the predicted size is 33.81. The size difference between the two predicted models is less than 4. Hence, the error percentage is insignificant, so both correlations are acceptable, but the modified Scherer is more compatible than others.

The BET test was performed to determine the specific surface area of the catalyst after calcination at 550 °C (Table 2). Whereas, the surface area of the perovskite catalysts is low, but its strong structure makes it valuable.

Figure 4 represents the hydrogen consumption of the catalyst after the calcination process. As reported in Fig. 4 there are two reduction peaks between 2000 and 4000 s. The current result is inline with previous studies<sup>11,32-34</sup>. The first reduction trend appears at low temperatures, roughly 280 °C in the 2500 s, while the second trend appears at temperatures between 380 and 430 °C in the 4200 s. Two peaks in the TPR profile reflect the two reducible cations in the B site (Fe and Co)<sup>11</sup>.

SEM images in Fig. 5a show that porous particles were formed and the EDXS proved that the actual composition of the catalyst is  $\text{LaFe}_{0.67}\text{Co}_{0.32}\text{O}_3$  (Fig. 5b).

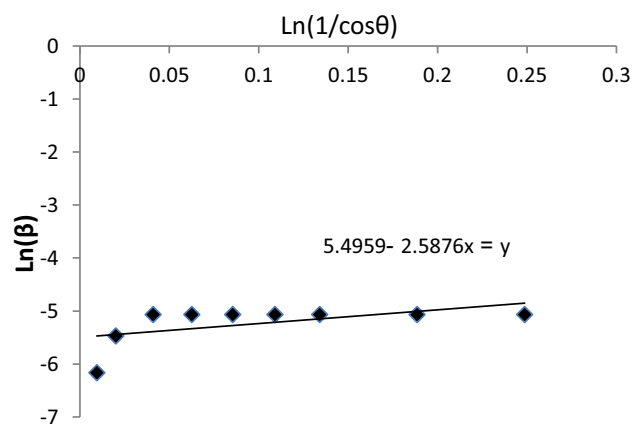


**Figure 3.**  $\ln\beta$  verses  $\ln(1/\cos\theta)$  based on XRD results.

	Surface area ( $\text{m}^2/\text{gr}$ )	Pore volume ( $\text{cm}^3/\text{gr}$ )	Pore size (nm)
$\text{LaFe}_{0.7}\text{Co}_{0.3}\text{O}_3$ (Fresh)	23.7	0.0959	24.2
$\text{LaFe}_{0.7}\text{Co}_{0.3}\text{O}_3$ (Used)	10.3	0.0625	27.6

**Table 2.** BET results.

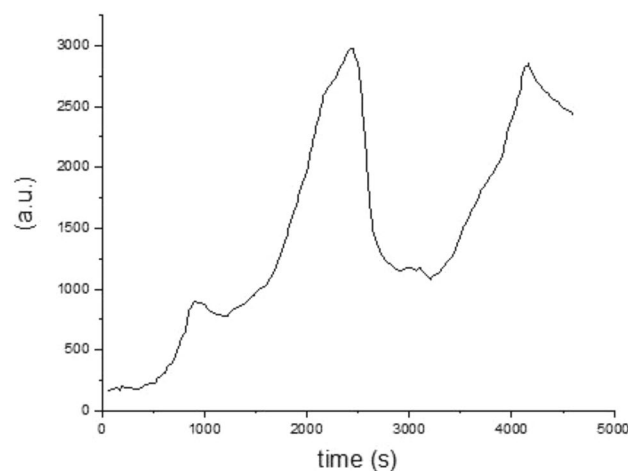


**Figure 4.** TPR profile of the perovskite catalyst.

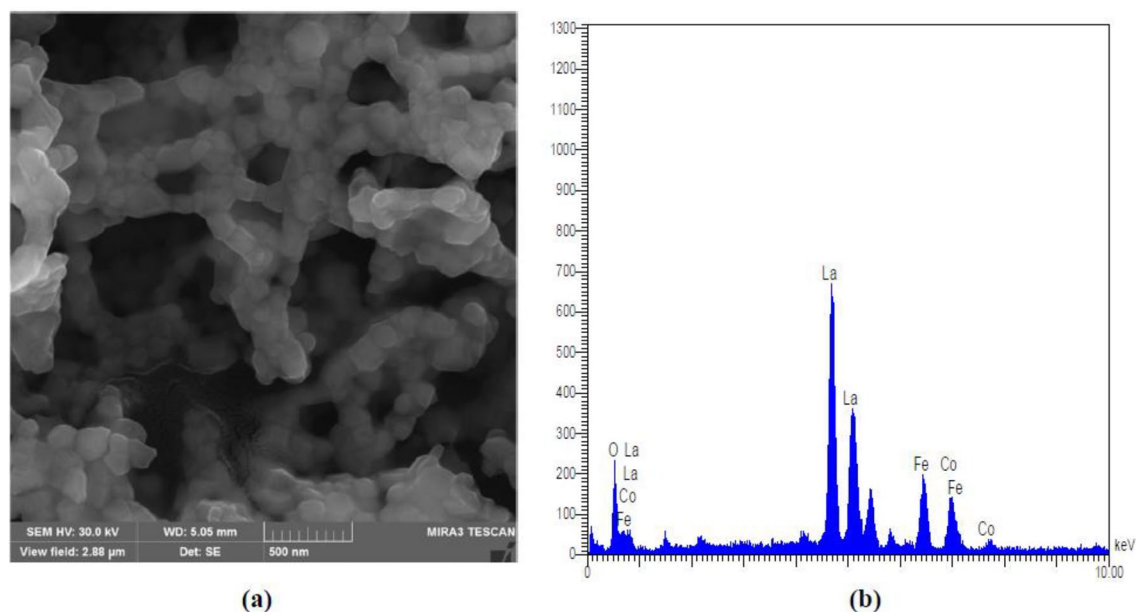


**Figure 5.** (a) SEM micrographs and (b) EDX Spectrum.

TEM observation of samples shows good distributions of grains of catalysts (Fig. 6). The results show that the particle size is between 20 and 140 nm, and the asymmetric shape of the grains proves that the XRD pattern is accurate.

### Kinetic model

The main goal of the current research is to develop an appropriate kinetic model to predict the behavior of the perovskite catalyst ( $\text{LaFe}_{0.7}\text{Co}_{0.3}\text{O}_3$ ) used for the Fischer–Tropsch process. The most crucial aspect of the FT process is elucidating the mechanism of the reaction. Moreover, the mechanisms were determined using various adsorption possibilities of CO and  $\text{H}_2$  molecules on the catalyst's surface. There are four mechanisms for FT synthesis, such as carbide, enolic, alkyl, and alkenyl<sup>23,35,36</sup>. However, the main difference between the mechanisms is the monomer formation; the monomer formation stage was used to estimate the reaction rate.

The activity of  $\text{LaFe}_{0.7}\text{Co}_{0.3}\text{O}_3$  perovskite catalyst was studied (Fig. 7) and the results show that after 50 h, the catalyst activity was stable. Additionally, in order to mitigate the impact of deactivation, new catalysts were loaded into each experiment. Therefore the kinetic data is reliable. The product selectivity at the temperature of 553 K and pressure of 20 bar within the catalyst activity range is reported (Fig. 8). The results show that the selectivity of  $\text{C}_5^+$  is in good agreement with previous studies<sup>8</sup>. Table 3 shows the elementary reaction sets for FT synthesis. The reaction rate expressions for the FTS based on elementary reactions are shown in Table 4. In the current study, to derive all reaction rates, represented in Table 5, the Langmuir–Hinshelwood–Hougen–Watson

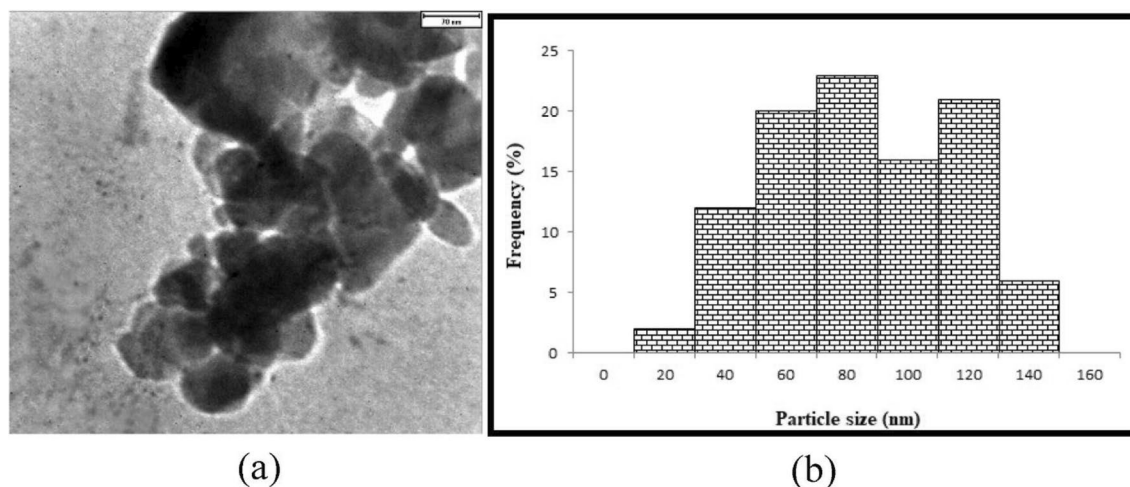


**Figure 6.** TEM Pattern (a) Schematic of catalyst, and (b) particle size distribution.

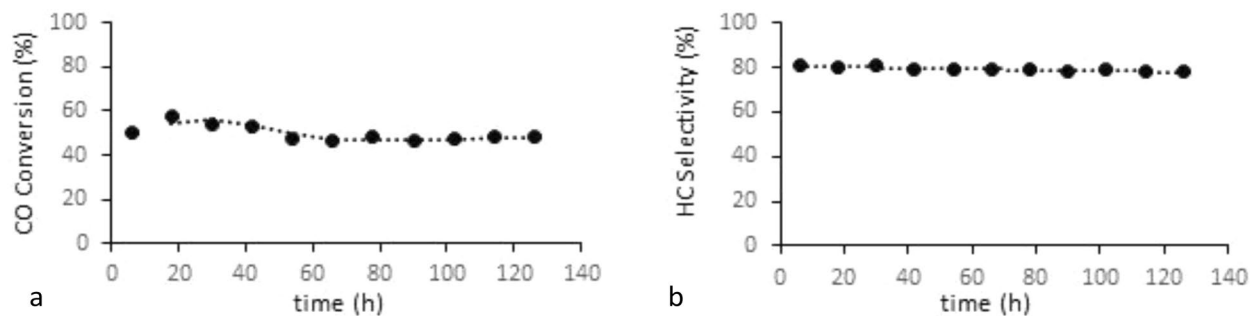


**Figure 7.** Activity diagram during the time (a) CO conversion (b) Hydrocarbon Selectivity.

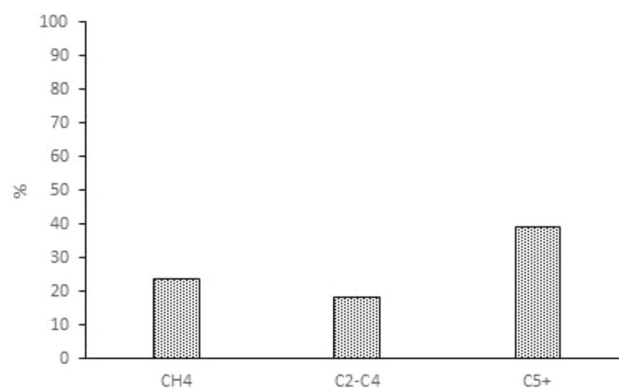


**Figure 8.** Product selectivity of LaFeCoO catalyst at a temperature of 553 K and pressure of 20 bar.

(LHHW) approach was applied accordingly. In addition, using polymath software, a suitable kinetic model was developed by fitting whole reaction rates against empirical data, and finally, the best kinetic model was chosen based on  $R^2$ ,  $R_{msd}$ , and MARR.

The most appropriate reaction rate ( $R^2$ ) should be close to 1. Moreover,  $R_{msd}$  and MARR might have a minimum value. The statistical parameters were determined as follows:

1. Square of the coefficient of correlation function ( $R^2$ ):

$$\sigma = \frac{1}{N_{exp}} \left( \sum_{i,CO}^{N_{exp}} r_{i,CO}^{exp} \right) \quad (7)$$

$$R^2 = 1 - \frac{\sum_{i=1}^{N_{exp}} (r_{i,CO}^{exp} - r_{i,CO}^{cal})^2}{\sum_{i=1}^{N_{exp}} (r_{i,CO}^{exp} - \sigma)^2} \quad (8)$$

2. Root Mean Square Deviation ( $R_{msd}$ )

$$R_{msd} = \frac{1}{N} \left( \sum_{i=1}^N (r_{i,CO}^{exp} - r_{i,CO}^{cal})^2 \right)^2 \quad (9)$$

3. Mean Absolute Relative Residual (MARR):

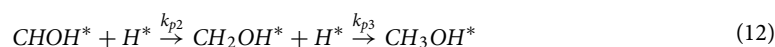
$$MARR = \sum_{i=1}^{N_{exp}} \left| \frac{r_{exp} - r_{cal}}{r_{exp}} \right| * \frac{100}{N_{exp}} \quad (10)$$

Comparing experimental data to the model equation demonstrates that the FT-VII (3) model is in good agreement with the empirical results. In this scenario, carbon monoxide and hydrogen atoms are reacted while adsorbed on the surface of a catalyst.



No	T(K)	H <sub>2</sub> /CO	P <sub>CO</sub> (bar)	P <sub>H<sub>2</sub></sub> (bar)	X <sub>CO</sub> (%)	X <sub>H<sub>2</sub></sub> (%)	-r <sub>CO</sub> *10 <sup>-3</sup> (mol/min. gr <sub>cat</sub> )
1	513.15	1.0	10.0	10.0	3.36	2.89	1.9699
2	513.15	2.0	3.3	6.7	11.15	20.74	2.1750
3	553.15	2.0	3.3	6.7	11.59	21.09	2.0976
4	553.15	1.0	5.0	5.0	7.02	6.18	1.9069
5	533.15	1.5	6.0	9.0	6.53	8.36	2.2094
6	553.15	2.0	6.7	13.3	6.69	12.71	2.4250
7	513.15	2.0	6.7	13.3	6.16	11.58	2.4085
8	533.15	1.0	10.0	10.0	3.59	3.12	2.0234
9	533.15	2.0	3.3	6.7	11.48	21.70	2.1557
10	573.15	2.0	3.3	6.7	11.97	22.74	2.0903
11	573.15	1.0	5.0	5.0	7.27	6.54	1.9061
12	553.15	1.5	6.0	9.0	6.76	9.15	2.2047
13	573.15	2.0	6.7	13.3	7.00	13.30	2.4495
14	533.15	2.0	6.7	13.3	6.47	12.23	2.4357
15	573.15	1.0	10.0	10.0	3.69	3.28	1.9376
16	553.15	1.0	7.5	7.5	4.84	4.16	1.9730
17	513.15	2.0	3.3	6.7	10.75	20.10	2.0981
18	553.15	1.0	5.0	5.0	6.99	6.22	1.9006
19	553.15	2.0	3.3	6.7	11.55	21.13	2.0900
20	533.15	1.5	6.0	9.0	6.47	8.35	2.1890
21	553.15	1.0	10.0	10.0	3.61	3.32	1.9621
22	513.15	2.0	3.3	6.7	11.06	20.68	2.1581
23	553.15	1.0	5.0	5.0	6.88	6.19	1.8706
24	553.15	2.0	3.3	6.7	11.55	21.13	2.0900
25	533.15	1.5	6.0	9.0	6.53	8.42	2.2090
26	533.15	1.5	6.0	9.0	6.64	8.76	2.2467
27	533.15	1.5	6.0	9.0	6.60	8.58	2.2325
28	533.15	1.5	6.0	9.0	6.53	8.55	2.2111
29	513.15	1.0	5.0	5.0	6.48	5.51	1.8980
30	503.15	2.0	6.7	13.3	5.86	10.84	2.3373
31	513.15	2.0	6.7	13.3	6.23	11.71	2.4355
32	513.15	1.0	10.0	10.0	3.36	2.89	1.9695
33	533.15	1.5	6.0	9.0	6.54	8.50	2.2131

**Table 3.** Experimental condition and results for kinetic tests.



All the reactions are series and have the same reaction rate. If the surface reaction controls the reaction rate, then the CO consumption rate is determined as below:

$$-r_{\text{CO}} = k_p \theta_{\text{CO}} \theta_{\text{H}} \quad (14)$$

and for H<sub>2</sub> surface adsorption:



$$k_{\text{ads,H}_2} P_{\text{H}_2} C_V^2 - k_{\text{des,H}_2} \theta_{\text{H}}^2 = 0 \quad (16)$$

$$b_{\text{H}_2} = \frac{k_{\text{ads,H}_2}}{k_{\text{des,H}_2}} \quad (17)$$

where  $b_{\text{H}_2}$  is equilibrium constant of H<sub>2</sub> adsorption step

$$\theta_{\text{H}} = (b_{\text{H}_2} P_{\text{H}_2})^{0.5} C_V \quad (18)$$

Model	No	Reaction scheme	Model	No	Reaction scheme
FT-I	1	$CO + * \leftrightarrow CO^*$	FT-X	1	$CO + * \leftrightarrow CO^*$
	2	$CO^* + H_2 \leftrightarrow CHOH^*$		2	$CO^* + * \leftrightarrow C^* + O^*$
	3	$CHOH^* + H_2 \leftrightarrow CH^* + H_2O$		3	$C^* + O^* + 2H_2 \leftrightarrow CH_3OH^* + *$
FT-II	1	$H_2 + * \leftrightarrow H_2^*$	FT-XI	4	$CH_3OH^* \leftrightarrow CH_2^* + H_2O$
	2	$CO + H_2^* \leftrightarrow CH_3OH^*$		1	$CO + * \leftrightarrow CO^*$
	3	$CH_3OH^* \leftrightarrow CH_2^* + H_2O$		2	$CO^* + * \leftrightarrow C^* + O^*$
FT-III	1	$H_2 + * \leftrightarrow H_2^*$	FT-XII	3	$C^* + O^* + H_2 \leftrightarrow CH_2^* + O^*$
	2	$CO + H_2^* \leftrightarrow CHOH^*$		4	$CH_2^* + O^* + H_2 \leftrightarrow CH_3OH^* + *$
	3	$CHOH^* + H_2 \leftrightarrow CH_3OH^*$		5	$CH_3OH^* \leftrightarrow CH_2^* + H_2O$
	4	$CH_3OH^* \leftrightarrow CH_2^* + H_2O$		1	$CO + 2^* \leftrightarrow C^* + O^*$
FT-IV	1	$H_2 + 2^* \leftrightarrow 2H^*$	FT-XIII	2	$H_2 + 2^* \leftrightarrow 2H^*$
	2	$CO + 4H^* \leftrightarrow CH_3OH^*$		3	$C^* + O^* + 4H^* \leftrightarrow CH_3OH^* + 2^*$
	3	$CH_3OH^* \leftrightarrow CH_2^* + H_2O$		4	$CH_3OH^* \leftrightarrow CH_2^* + H_2O$
FT-V	1	$H_2 + 2^* \leftrightarrow 2H^*$	FT-XIV	1	$CO + 2^* \leftrightarrow C^* + O^*$
	2	$CO + 2H^* \leftrightarrow CHOH^*$		2	$H_2 + * \leftrightarrow H_2^*$
	3	$CHOH^* + H_2 \leftrightarrow CH_3OH^*$		3	$C^* + O^* + H_2^* \leftrightarrow CH_2^* + O^* + *$
	4	$CH_3OH^* \leftrightarrow CH_2^* + H_2O$		4	$CH_2^* + O^* + 2H^* \leftrightarrow CH_3OH^* + 2^*$
FT-VI	1	$H_2 + 2^* \leftrightarrow 2H^*$	FT-XV	5	$CH_3OH^* \leftrightarrow CH_2^* + H_2O$
		$CO + 2H^* \leftrightarrow COH^*$		1	$CO + 2^* \leftrightarrow C^* + O^*$
		$CHO^* + H^* \leftrightarrow CH_2OH^* + *$		2	$H_2 + * \leftrightarrow H_2^*$
		$CH_2OH^* + H^* \leftrightarrow CH_3OH^* + *$		3	$C^* + O^* + H_2^* \leftrightarrow CH_2^* + O^* + *$
		$CH_3OH^* \leftrightarrow CH_2^* + H_2O$		4	$CH_2^* + O^* + H_2^* \leftrightarrow CH_3OH^* + 2^*$
FT-VII	1	$CO + * \leftrightarrow CO^*$	FT-XVI	5	$CH_3OH^* \leftrightarrow CH_2^* + H_2O$
	2	$H_2 + 2^* \leftrightarrow 2H^*$		1	$CO + 2^* \leftrightarrow C^* + O^*$
	3	$CO + H^* \leftrightarrow CHO^* + *$		2	$C^* + H_2 \leftrightarrow CH_2^* + *$
	4	$CHO^* + H^* \leftrightarrow CHOH^* + *$		1	$CO + 2^* \leftrightarrow C^* + O^*$
	5	$CHOH^* + H^* \leftrightarrow CH_2OH^* + *$		2	$H_2 + 2^* \leftrightarrow 2H^*$
	6	$CH_2OH^* + H^* \leftrightarrow CH_3OH^* + *$		3	$C^* + H^* \leftrightarrow CH^* + *$
	7	$CH_3OH^* \leftrightarrow CH_2^* + H_2O$		4	$CH^* + H^* \leftrightarrow CH_2^*$
FT-VIII	1	$CO + * \leftrightarrow CO^*$	FT-XVII	1	$CO + 2^* \leftrightarrow C^* + O^*$
	2	$H_2 + 2^* \leftrightarrow 2H^*$		2	$H_2 + * \leftrightarrow H_2^*$
	3	$CO^* + 4H^* \leftrightarrow CH_3OH^* + *$		3	$C^* + H_2^* \leftrightarrow CH_2^* + *$
	4	$CH_3OH^* \leftrightarrow CH_2^* + H_2O$		1	$CO + 2^* \leftrightarrow C^* + O^*$
FT-IX	1	$CO + * \leftrightarrow CO^*$	FT-XVIII	1	$CO + 2^* \leftrightarrow C^* + O^*$
	2	$H_2 + 2^* \leftrightarrow 2H^*$		2	$H_2 + 2^* \leftrightarrow 2H^*$
	3	$CO^* + H_2 \leftrightarrow CH_2O^* + *$		3	$C^* + 2H^* \leftrightarrow CH_2^* + *$
	4	$CH_2O^* + H_2^* \leftrightarrow CH_3OH^* + *$			
	5	$CH_3OH^* \leftrightarrow CH_2^* + H_2O$			

**Table 4.** Elementary reaction sets for Fischer–Tropsch synthesis.

$$\theta_{CO} = b_{CO}P_{CO}C_V \quad (19)$$

$$C_V = 1 - \sum \theta = 1 - (\theta_{CO} + \theta_H) \quad (20)$$

$$C_V = 1 - (b_{CO}P_{CO} + (b_{H_2}P_{H_2})^{0.5})C_V \quad (21)$$

$$C_V = \frac{1}{1 + (b_{CO}P_{CO} + (b_{H_2}P_{H_2})^{0.5})} \quad (22)$$

Finally the CO consumption rate is obtained as below:

$$-r_{CO} = \frac{k_p b_{CO} P_{CO} (b_{H_2} P_{H_2})^{0.5}}{(1 + b_{CO} P_{CO} + (b_{H_2} P_{H_2})^{0.5})^2} \quad (23)$$

Model	Rate equation	Model	Rate equation
FT-I (1)	$-r_{CO} = \frac{k \cdot b_{CO} \cdot P_{CO} \cdot P_{H_2}}{1 + b_{CO} \cdot P_{CO}}$	FT-X (1)	$-r_{CO} = \frac{k_{CO} \cdot b_{CO} \cdot P_{CO}}{\left(1 + 2(b_{CO} \cdot P_{CO})^{\frac{1}{2}}\right)^2}$
FT-I (2)	$-r_{CO} = \frac{k \cdot b_{CO} \cdot P_{CO}}{1 + b_{CO} \cdot P_{CO}}$	FT-X (2)	$-r_{CO} = \frac{k_{CO} \cdot b_{CO} \cdot P_{CO} \cdot (P_{H_2})^2}{\left(1 + 2(b_{CO} \cdot P_{CO})^{\frac{1}{2}}\right)^2}$
FT-II (1)	$-r_{CO} = \frac{k_{H_2} \cdot b_{H_2} \cdot P_{H_2}}{1 + b_{H_2} \cdot P_{H_2}}$	FT-XI	$-r_{CO} = \frac{k_{CO} \cdot b_{CO} \cdot P_{CO} \cdot P_{H_2}}{\left(1 + 2(b_{CO} \cdot P_{CO})^{\frac{1}{2}}\right)^2}$
FT-II (2)	$-r_{CO} = \frac{k_{H_2} \cdot P_{CO} \cdot (b_{H_2} \cdot P_{H_2})^2}{(1 + b_{H_2} \cdot P_{H_2})^2}$	FT-XII (1)	$-r_{CO} = \frac{k_{CO} \cdot b_{CO} \cdot P_{CO}}{\left(1 + 2(b_{CO} \cdot P_{CO})^{\frac{1}{2}} \cdot (b_{H_2} \cdot P_{H_2})^{\frac{1}{2}}\right)^2}$
FT-III	$-r_{CO} = \frac{k \cdot P_{CO} \cdot b_{H_2} \cdot P_{H_2}}{1 + b_{H_2} \cdot P_{H_2}}$	FT-XII (2)	$-r_{CO} = \frac{k_{H_2} \cdot b_{H_2} \cdot P_{H_2}}{\left(1 + 2(b_{CO} \cdot P_{CO})^{\frac{1}{2}} \cdot (b_{H_2} \cdot P_{H_2})^{\frac{1}{2}}\right)^2}$
FT-IV (1)	$-r_{CO} = \frac{k \cdot P_{CO} \cdot b_{H_2} \cdot P_{H_2}}{\left(1 + (b_{H_2} \cdot P_{H_2})^{\frac{1}{2}}\right)^4}$	FT-XII (3)	$-r_{CO} = \frac{k \cdot b_{CO} \cdot P_{CO} \cdot (b_{H_2} \cdot P_{H_2})^2}{\left(1 + 2(b_{CO} \cdot P_{CO})^{\frac{1}{2}} \cdot (b_{H_2} \cdot P_{H_2})^{\frac{1}{2}}\right)^6}$
FT-IV (2)	$-r_{CO} = \frac{k \cdot P_{CO} \cdot (b_{H_2} \cdot P_{H_2})^2}{(1 + (b_{H_2} \cdot P_{H_2})^{\frac{1}{2}})^4}$	FT-XIII	$-r_{CO} = \frac{k \cdot b_{CO} \cdot P_{CO} \cdot b_{H_2} \cdot P_{H_2}}{(1 + 2(b_{CO} \cdot P_{CO})^{\frac{1}{2}} \cdot (b_{H_2} \cdot P_{H_2})^{\frac{1}{2}})^4}$
FT-V	$-r_{CO} = \frac{k \cdot P_{CO} \cdot b_{H_2} \cdot P_{H_2}}{\left(1 + (b_{H_2} \cdot P_{H_2})^{\frac{1}{2}}\right)^2}$	FT-XIV (1)	$-r_{CO} = \frac{k_{CO} \cdot b_{CO} \cdot P_{CO}}{\left(1 + 2(b_{CO} \cdot P_{CO})^{\frac{1}{2}} + b_{H_2} \cdot P_{H_2}\right)^2}$
FT-VI	$-r_{CO} = \frac{k \cdot P_{CO} \cdot (b_{H_2} \cdot P_{H_2})^{1/2}}{1 + (b_{H_2} \cdot P_{H_2})^{1/2}}$	FT-XIV (2)	$-r_{CO} = \frac{k_{H_2} \cdot b_{H_2} \cdot P_{H_2}}{\left(1 + 2(b_{CO} \cdot P_{CO})^{\frac{1}{2}} + b_{H_2} \cdot P_{H_2}\right)^2}$
FT-VII (1)	$-r_{CO} = \frac{k_{CO} \cdot b_{CO} \cdot P_{CO}}{\left(1 + b_{CO} \cdot P_{CO} + (b_{H_2} \cdot P_{H_2})^{\frac{1}{2}}\right)}$	FT-XIV (3)	$-r_{CO} = \frac{k \cdot b_{CO} \cdot P_{CO} \cdot b_{H_2} \cdot P_{H_2}}{\left(1 + 2(b_{CO} \cdot P_{CO})^{\frac{1}{2}} + b_{H_2} \cdot P_{H_2}\right)^3}$
FT-VII (2)	$-r_{CO} = \frac{k_{H_2} \cdot b_{H_2} \cdot P_{H_2}}{\left(1 + b_{CO} \cdot P_{CO} + (b_{H_2} \cdot P_{H_2})^{\frac{1}{2}}\right)^2}$	FT-XV (1)	$-r_{CO} = \frac{k \cdot (b_{CO} \cdot P_{CO})^{1/2} \cdot P_{H_2}}{\left(1 + 2(b_{CO} \cdot P_{CO})^{\frac{1}{2}}\right)^2}$
FT-VII (3)	$-r_{CO} = \frac{k \cdot b_{CO} \cdot P_{CO} \cdot (b_{H_2} \cdot P_{H_2})^{1/2}}{\left(1 + b_{CO} \cdot P_{CO} + (b_{H_2} \cdot P_{H_2})^{\frac{1}{2}}\right)^2}$	FT-XV (2)	$-r_{CO} = \frac{k \cdot (b_{CO} \cdot P_{CO})^{1/2} \cdot P_{H_2}}{1 + 2(b_{CO} \cdot P_{CO})^{1/2}}$
FT-VIII	$-r_{CO} = \frac{k \cdot b_{CO} \cdot P_{CO} \cdot (b_{H_2} \cdot P_{H_2})^2}{(1 + b_{CO} \cdot P_{CO} + b_{H_2} \cdot P_{H_2})^2}$	FT-XVI	$-r_{CO} = \frac{k \cdot (b_{CO} \cdot P_{CO})^{1/2} \cdot (b_{H_2} \cdot P_{CO})^{1/2}}{\left(1 + 2(b_{CO} \cdot P_{CO})^{\frac{1}{2}} + (b_{H_2} \cdot P_{H_2})^{\frac{1}{2}}\right)^2}$
FT-IX (1)	$-r_{CO} = \frac{k_{CO} \cdot b_{CO} \cdot P_{CO}}{1 + b_{CO} \cdot P_{CO} + b_{H_2} \cdot P_{H_2}}$	FT-XVII	$-r_{CO} = \frac{k \cdot (b_{CO} \cdot P_{CO})^{1/2} \cdot b_{H_2} \cdot P_{CO}}{\left(1 + 2(b_{CO} \cdot P_{CO})^{\frac{1}{2}} + b_{H_2} \cdot P_{H_2}\right)^2}$
FT-IX (2)	$-r_{CO} = \frac{k_{H_2} \cdot b_{H_2} \cdot P_{H_2}}{1 + b_{CO} \cdot P_{CO} + b_{H_2} \cdot P_{H_2}}$	FT-XVIII	$-r_{CO} = \frac{k \cdot (b_{CO} \cdot P_{CO})^{1/2} \cdot b_{H_2} \cdot P_{CO}}{\left(1 + 2(b_{CO} \cdot P_{CO})^{\frac{1}{2}} + (b_{H_2} \cdot P_{H_2})^{\frac{1}{2}}\right)^3}$
FT-IX (3)	$-r_{CO} = \frac{k \cdot b_{CO} \cdot P_{CO} \cdot b_{H_2} \cdot P_{H_2}}{(1 + b_{CO} \cdot P_{CO} + b_{H_2} \cdot P_{H_2})^2}$		

**Table 5.** Reaction rates for Fischer–Tropsch synthesis.

The constant coefficient and validation parameters are estimated and presented in Table 6. The MARR percentage of the FT-VII(3) model is 9.65. The model, however, shows less deviation from the experimental data and is consistent with it. The MARR% values of the other obtained kinetic models are presented in Table 7; as it was shown, the FT-VII(3) model having the minimal MARR value fits the experimental data well. The best-fitted kinetic model is an enolic mechanism; in this mechanism, the base component (CHOH) is formed by partial

Parameters	Value
$K_0$ (mol/min.g <sub>cat.</sub> )	0.01756
$E_a$ (kJ/mol)	106.25
$b_{CO}$ (1/bar)	0.4994
$b_{H_2}$ (1/bar)	0.1203
$R^2$	0.9728
MARR (%)	9.65

**Table 6.** Values of kinetic parameters of FT-VII(3) model.

Kinetic model	$k/b_{CO}, b_{H_2}$	MARR%	Kinetic model	$k/b_{CO}, b_{H_2}$	MARR%
FT-I (1)	$1.47E-1/14.84E0/1.47E-1$	42	FT-X (1)	$9.05E-3/49.88E0/-$	10.8
FT-I (2)	$2.16E-3/14.84E0/-$	10.3	FT-X (2)	$9.92E-2/2.57E-5/-$	53.7
FT-II (1)	$2.64E-3/-/5.21E-1$	14.3	FT-XI	$3.97E-3/2.91E-2/-$	34.3
FT-II (2)	$2.49E-4/1010.70E0$	32.6	FT-XII (1)	$5.46E-1/2.59E-3/1.87E0$	20.3
FT-III	$1.44E-4/-/101.96E0$	59.3	FT-XII (2)	$7.75E-1/9.47E-5/2.7E0$	10.69
FT-IV (1)	$9.63E-3/-/1.11E0$	29.4	FT-XII (3)	$2.15E0/1.49E-1/2.89E-2$	10.49
FT-IV (2)	$1.42E-3/-/4.67E-1$	37.2	FT-XIII	$1.43E-1/6.63E-2/6.64E-2$	11.46
FT-V	$4.94E-4/-/1.50E0$	32.9	FT-XIV (1)	$9.15E-3/1.50E0/2.61E-1$	54.7
FT-VI	$5.46E-2/-/3.33E-6$	34.8	FT-XIV (2)	$1.33E-2/8.11E-2/5.88E-3$	13.1
FT-VII (1)	$3.12E-3/3.04E0/1.10E0$	18.6	FT-XIV (3)	$6.68E-2/1.69E0/101.9E0$	10.3
FT-VII (2)	$5.64E-3/5.56E-1/6.23E-2$	18.3	FT-XV (1)	$2.38E-2/102.0E0/-$	13.0
FT-VII (3)	$1.86E0/4.99E-1/1.20E-1$	9.65	FT-XV (2)	$2.31E0/1.36E-9/-$	33.5
FT-VIII	$1.18E-4/9.06E0/8.24E0$	22.1	FT-XVI	$2.77E-1/5.10E-1/9.86E-4$	12.81
FT-IX (1)	$1.99E-3/1.06E0/1.70E0$	13.0	FT-XVII	$25.0E0/2.50E-4/2.01E0$	18.9
FT-IX (2)	$3.11E-3/5.80E-1/2.06E-1$	12.4	FT-XVIII	$72.66E0/7.16E-4/2.01E0$	9.96
FT-IX (3)	$9.79E-1/5.87E-2/3.63E-3$	29.4			

**Table 7.** Parameters and mean absolute relative residuals (MARR) for the FT kinetic models.

hydrogenation of the absorbed carbon monoxide. According to previous research<sup>42,43</sup>, the enolic mechanism is much better than the carbide mechanism for bimetallic oxide catalysts.

In addition, Fig. 9 depicts the comparison between experimental data and the calculated CO consumption rate. Polymath software shows that the experimental and calculated rates were close together and at some point, the experimental and calculated data were overlapped.

The reaction rate is determined using the model equation and compared with the empirical data (Fig. 10a and b). The compatibility between the model and the experimental data is demonstrated by the closeness of the data to the straight line and the symmetry shape around the straight line.

In addition, Fig. 10b presents the calculated against the experimental reaction rate, and it shows that the calculated reaction rate is acceptable for predicting Fischer–Tropsch synthesis. The activation energy of a reaction is obtained by fitting data with the Arrhenius equation in various conditions. The activation energy of hydrocarbon formation is mostly between 75 to 110 kJ/mol<sup>37–39</sup>. In the current study, the activation energy value is 106.25 kJ/mol, which is close to activation energy reported previously 106.2 kJ/mol by abdollahi et al. and 100 and 103 kJ/mol yange et al. and storch et al.<sup>40–42</sup>. Nevertheless, it was substantially higher than the value of 80.63 and 66.01 kJ/mol which are reported by davies et al.<sup>43</sup> and mansouri et al.<sup>16</sup>. Although the activation energy shows the importance of the diffusion interface, the high activation energies indicate the absence of diffusion effects in the Fischer–Tropsch reaction. Therefore, the pore diffusion restriction led to the low activation energy in the Fischer–Tropsch reaction. The pore size and catalyst structure correspond with the catalyst's preparation method and component<sup>16,44</sup>.

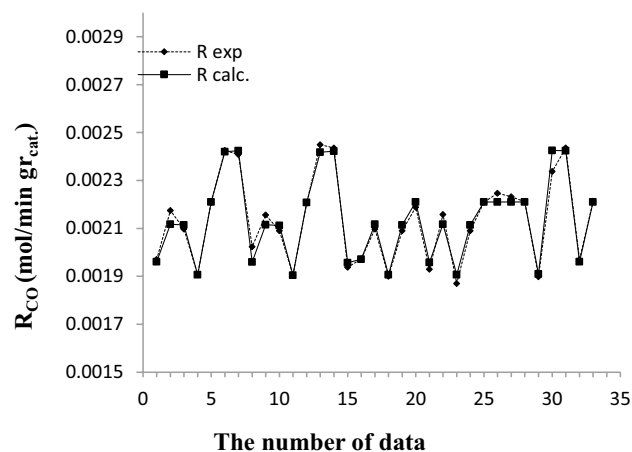


**Figure 9.** The difference between experimental and calculated reaction rate.

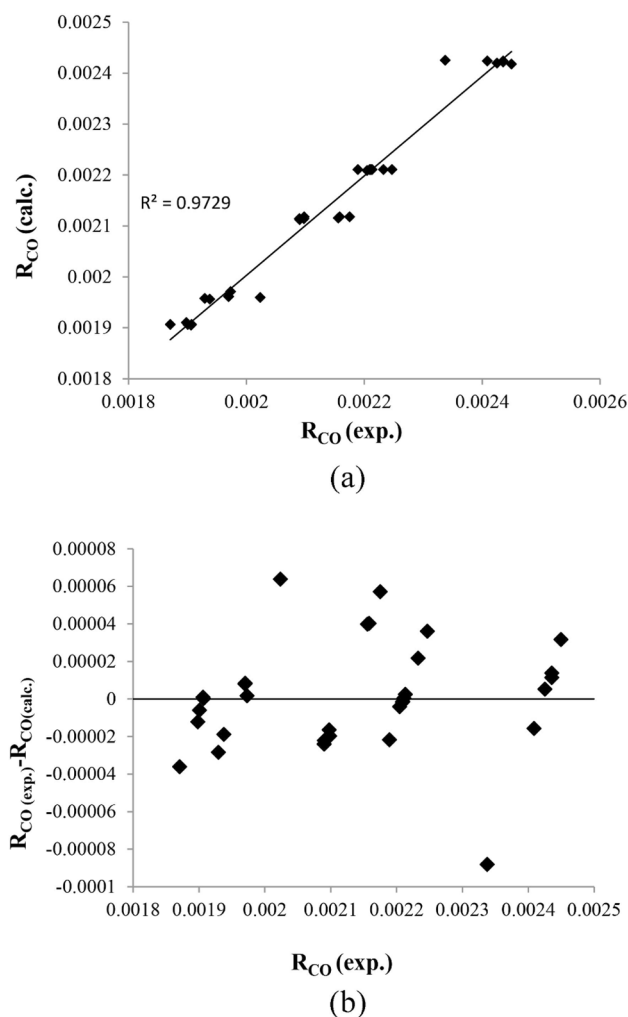


**Figure 10.** The calculated vs. the experimental reaction rate (a) normal plot, (b) residual plot.

## Conclusion

The performance of  $\text{LaFe}_{0.7}\text{Co}_{0.3}\text{O}_3$  perovskite catalyst and kinetic of Fischer–Tropsch synthesis (CO conversion) were investigated in a fixed bed reactor under various operating conditions (e.g.  $\text{H}_2/\text{CO}$ : 1–2, pressure: 10–20 barg, temperature: 240–300 °C, and GHSV: 3000 1/h). Several Langmuir–Hinshelwood–Hougen–Watson (LHHW) rate equations were derived. The unknown kinetic parameters such as  $R^2$ ,  $R_{\text{msd}}$ , and MARR were estimated using empirical data in Polymath software. In addition, the kinetic parameters were estimated with non-linear regression and the results show that the FT-VII model predicts CO consumption with high compatibility. Finally, the activation energy was determined with respect to the Arrhenius equation and the optimum value of 106.25 kJ/mol was estimated under various operating conditions. The kinetic parameters correspond with the preparation method and catalyst component. Therefore, the perovskite catalyst is activated at a higher temperature, and consequently, the coking issue is diminished during the operation.

## Data availability

All experimental data were published in the current article. The additional data and information will be provided to individuals upon official request to the corresponding author [Seyed Hasan Hashemabadi].

Received: 18 July 2023; Accepted: 12 April 2024

Published online: 22 April 2024

## References

1. Eschemann, T. O. & de Jong, K. P. Deactivation behavior of Co/TiO<sub>2</sub> catalysts during Fischer–Tropsch synthesis. *ACS Catal.* **5**(6), 3181–3188 (2015).
2. Wang, Z. *et al.* Effect of steam during Fischer–Tropsch synthesis using biomass-derived syngas. *Catal. Lett.* **147**, 62–70 (2017).
3. Okoye-Chine, C. G. *et al.* A critical review of the impact of water on cobalt-based catalysts in Fischer–Tropsch synthesis. *Fuel Process. Technol.* **192**, 105–129 (2019).
4. Wang, D. *et al.* Cobalt-based Fischer–Tropsch synthesis: Effect of the catalyst granule thermal conductivity on the catalytic performance. *Mol. Catal.* **502**, 111395 (2021).

5. Zhao, X. *et al.* Comparison of preparation methods of iron-based catalysts for enhancing Fischer-Tropsch synthesis performance. *Mol. Catal.* **449**, 99–105 (2018).
6. Abrokwah, R. Y. *et al.* Effect of titania support on Fischer-Tropsch synthesis using cobalt, iron, and ruthenium catalysts in silicon-microchannel microreactor. *Mol. Catal.* **478**, 110566 (2019).
7. Teimouri, Z., Abatzoglou, N. & Dalai, A. K. Kinetics and selectivity study of Fischer-Tropsch synthesis to C5+ hydrocarbons: A review. *Catalysts* **11**(3), 330 (2021).
8. Bedel, L. *et al.* La (1–y) Co<sub>0.4</sub>Fe<sub>0.6</sub>O<sub>3–δ</sub> perovskite oxides as catalysts for Fischer-Tropsch synthesis. *J. Catal.* **235**(2), 279–294 (2005).
9. Tejuca, L. G. & Fierro, J. L. *Properties and Applications of Perovskite-Type Oxides* (CRC Press, 2000).
10. Wang, Z. J. *et al.* Surface science studies on cobalt Fischer-Tropsch catalysts. *ChemCatChem* **3**(3), 551–559 (2011).
11. Ao, M. *et al.* Structure and activity of strontium substituted LaCoO<sub>3</sub> perovskite catalysts for syngas conversion. *J. Mol. Catal. A Chem.* **416**, 96–104 (2016).
12. Jacobs, R. *et al.* Assessing correlations of perovskite catalytic performance with electronic structure descriptors. *Chem. Mater.* **31**(3), 785–797 (2019).
13. Das, T. K. *et al.* Fischer-Tropsch synthesis: Kinetics and effect of water for a Co/Al<sub>2</sub>O<sub>3</sub> catalyst. In *Fischer-Tropsch Synthesis, Catalysts and Catalysis* (ed. Davis, B. H.) 289–314 (Elsevier, 2007).
14. Das, T. K. *et al.* Fischer-Tropsch synthesis: Kinetics and effect of water for a Co/SiO<sub>2</sub> catalyst. *Energy Fuels* **19**(4), 1430–1439 (2005).
15. Rautavuoma, A. O. & Van der Baan, H. Kinetics and mechanism of the Fischer-Tropsch hydrocarbon synthesis on a cobalt on alumina catalyst. *Appl. Catal. (Netherlands)* **1**(5), 247–272 (1981).
16. Mansouri, M. *et al.* Kinetics studies of nano-structured cobalt-manganese oxide catalysts in Fischer-Tropsch synthesis. *J. Ind. Eng. Chem.* **19**(4), 1177–1183 (2013).
17. Zennaro, R., Tagliabue, M. & Bartholomew, C. H. Kinetics of Fischer-Tropsch synthesis on titania-supported cobalt. *Catal. Today* **58**(4), 309–319 (2000).
18. Yates, I. C. & Satterfield, C. N. Intrinsic kinetics of the Fischer-Tropsch synthesis on a cobalt catalyst. *Energy Fuels* **5**(1), 168–173 (1991).
19. Dry, M. E. Advances in Fischer-Tropsch chemistry. *Ind. Eng. Chem. Prod. Res. Dev.* **15**(4), 282–286 (1976).
20. Botes, F. G. & Breman, B. B. Development and testing of a new macro kinetic expression for the iron-based low-temperature Fischer-Tropsch reaction. *Ind. Eng. Chem. Res.* **45**(22), 7415–7426 (2006).
21. Botes, F. G., van Dyk, B. & McGregor, C. The development of a macro kinetic model for a commercial Co/Pt/Al<sub>2</sub>O<sub>3</sub> Fischer-Tropsch catalyst. *Ind. Eng. Chem. Res.* **48**(23), 10439–10447 (2009).
22. Ojeda, M. *et al.* CO activation pathways and the mechanism of Fischer-Tropsch synthesis. *J. Catal.* **272**(2), 287–297 (2010).
23. Nikbakht, N., Mirzaei, A. A. & Atashi, H. Kinetic modeling of the Fischer-Tropsch reaction over a zeolite supported Fe-Co-Ce catalyst prepared using impregnation procedure. *Fuel* **229**, 209–216 (2018).
24. Einbeigi, A. *et al.* Development of new comprehensive kinetic models for Fischer-Tropsch synthesis process over Fe-Co/γ-Al<sub>2</sub>O<sub>3</sub> nanocatalyst in a fixed-bed reactor. *J. Taiwan Inst. Chem. Eng.* **103**, 57–66 (2019).
25. Yahyazadeh, A. *et al.* Comprehensive kinetic study for Fischer-Tropsch reaction over KMoFe/CNTs nano-structured catalyst. *Can. J. Chem. Eng.* **101**(6), 3132–52 (2023).
26. Liu, Z. *et al.* Structural and microstructural effects of Mo<sup>3+</sup>/Mo<sup>5+</sup> codoping on properties and photocatalytic performance of nanostructured TiO<sub>2</sub> thin films. *J. Phys. Chem. C* **123**(18), 11781–11790 (2019).
27. Mohammadi, M. *et al.* Synthesis of high surface area nanocrystalline anatase-TiO<sub>2</sub> powders derived from particulate sol-gel route by tailoring processing parameters. *J. Sol-gel Sci. Technol.* **40**(1), 15–23 (2006).
28. Cordero-Cabrera, M., Walker, G. & Grant, D. Effect of processing parameters on the particle size and stabilisation of Titania sols. *J. Mater. Sci.* **40**(14), 3709–3714 (2005).
29. Sie, S., Senden, M. & Van Wechem, H. Conversion of natural gas to transportation fuels via the shell middle distillate synthesis process (SMDS). *Catal. Today* **8**(3), 371–394 (1991).
30. Kellner, C. S. & Bell, A. T. The kinetics and mechanism of carbon monoxide hydrogenation over alumina-supported ruthenium. *J. Catal.* **70**(2), 418–432 (1981).
31. Monshi, A., Foroughi, M. R. & Monshi, M. R. Modified Scherrer equation to estimate more accurately nano-crystallite size using XRD. *World J. Nano Sci. Eng.* **2**(3), 154–160 (2012).
32. Bedel, L. *et al.* Co<sub>0</sub> from partial reduction of La (Co, Fe) O<sub>3</sub> perovskites for Fischer-Tropsch synthesis. *Catal. Today* **85**(2–4), 207–218 (2003).
33. Escalona, N., Fuentealba, S. & Pecchi, G. Fischer-Tropsch synthesis over LaFe<sub>1–x</sub>Co<sub>x</sub>O<sub>3</sub> perovskites from a simulated biosyngas feed. *Appl. Catal. A Gen.* **381**(1–2), 253–260 (2010).
34. Liu, G. *et al.* Bi-metal Cu–Co from LaCo<sub>1–x</sub>Cu<sub>x</sub>O<sub>3</sub> perovskite supported on zirconia for the synthesis of higher alcohols. *Fuel Process. Technol.* **128**, 289–296 (2014).
35. Sun, Y. *et al.* Fischer-Tropsch synthesis using iron based catalyst in a microchannel reactor: Performance evaluation and kinetic modeling. *Int. J. Hydrogen Energy* **42**(49), 29222–29235 (2017).
36. Mousavi, S. *et al.* Generalized kinetic model for iron and cobalt based Fischer-Tropsch synthesis catalysts: Review and model evaluation. *Appl. Catal. A Gen.* **506**, 57–66 (2015).
37. Lox, E. S. & Froment, G. F. Kinetics of the Fischer-Tropsch reaction on a precipitated promoted iron catalyst. 2. Kinetic modeling. *Ind. Eng. Chem. Res.* **32**(1), 71–82 (1993).
38. Huff, G. A. Jr. & Satterfield, C. N. Liquid accumulation in catalyst pores in a Fischer-Tropsch fixed-bed reactor. *Ind. Eng. Chem. Process Des. Dev.* **24**(4), 986–995 (1985).
39. Dictor, R. A. & Bell, A. T. Fischer-Tropsch synthesis over reduced and unreduced iron oxide catalysts. *J. Catal.* **97**(1), 121–136 (1986).
40. Yang, C.-H., Massoth, F. & Oblad, A. *Kinetics of CO+ H<sub>2</sub> Reaction Over Co-Cu-Al<sub>2</sub>O<sub>3</sub> Catalyst* (ACS Publications, 1979).
41. Abdollahi, M. *et al.* Fischer-Tropsch study over impregnated silica-supported cobalt-iron nanocatalyst. *J. Iran. Chem. Soc.* **14**, 245–256 (2017).
42. Storch, H.H., Golombic, N., Anderson, R.B. The Fischer-Tropsch and related syntheses: including a summary of theoretical and applied contact catalysis. (1951).
43. Davies, I. & Möller, K. P. Development of a kinetic model for low temperature Fischer-Tropsch synthesis. *Chem. Eng. Sci.* **241**, 116666 (2021).
44. Sari, A., Zamani, Y. & Taheri, S. A. Intrinsic kinetics of Fischer-Tropsch reactions over an industrial Co–Ru/γ-Al<sub>2</sub>O<sub>3</sub> catalyst in slurry phase reactor. *Fuel Process. Technol.* **90**(10), 1305–1313 (2009).

## Author contributions

All authors contributed to the study conception and design. Material preparation, data collection and experiments analysis were performed by Behnoosh Moshtari And Yahya Zamani. Behnoosh Moshtari and Seyed Hashemabadi investigated the mechanism and derived kinetic model. The first draft of the manuscript was

written by Behnoosh Moshtari and all authors commented on previous versions of the manuscript. All authors read and approved the final manuscript.

### Competing interests

The authors declare no competing interests.

### Additional information

**Correspondence** and requests for materials should be addressed to S.H.H.

**Reprints and permissions information** is available at [www.nature.com/reprints](http://www.nature.com/reprints).

**Publisher's note** Springer Nature remains neutral with regard to jurisdictional claims in published maps and institutional affiliations.



**Open Access** This article is licensed under a Creative Commons Attribution 4.0 International License, which permits use, sharing, adaptation, distribution and reproduction in any medium or format, as long as you give appropriate credit to the original author(s) and the source, provide a link to the Creative Commons licence, and indicate if changes were made. The images or other third party material in this article are included in the article's Creative Commons licence, unless indicated otherwise in a credit line to the material. If material is not included in the article's Creative Commons licence and your intended use is not permitted by statutory regulation or exceeds the permitted use, you will need to obtain permission directly from the copyright holder. To view a copy of this licence, visit <http://creativecommons.org/licenses/by/4.0/>.

© The Author(s) 2024